Live-Load Performance Evaluation of Historic Covered Timber Bridges in the United States

Junwon Seo, Ph.D., P.E., M.ASCE[1]; Travis K. Hosteng, P.E., M.ASCE[2]; Brent M. Phares, Ph.D., P.E., M.ASCE[3]; and James P. Wacker, P.E., M.ASCE[4]

Abstract: The National Historic Covered Bridge Preservation Program (NHCBP), sponsored by the Federal Highway Administration (FHWA), was established to preserve the covered timber bridge structures that were constructed in the early 1800s. Today, many of the approximately 880 covered timber bridges still in existence in the United States are closed to vehicular traffic; furthermore, a large percentage of the remaining bridges open to traffic are restricted by load postings. Unfortunately, there are no current load-rating standards for covered timber bridges, so engineers do not have many resources at their disposal to reliably understand the behavior of these complex structures. As a result, the estimated load postings and/or ratings are often too conservative. To better understand the live-load performance of covered timber bridges and to develop improved criteria for their load ratings, a series of live-load tests were performed on 11 single-span, historic covered timber bridges. This paper explains the field testing conducted on all of the bridges, and makes recommendations for the conduct of other similar tests. The tests consisted of installing a network of multiple displacement and strain sensors on the structures, and monitoring global displacements and member strains at various cross sections during passage of a known test. The vehicle used in the testing met the load restrictions in place at the time of testing. The results of this work serve as a basis for instrumentation and field testing, to investigate the live-load performance on such bridges. This paper outlines the field-testing methods and summarizes the results from the testing of all 11 bridges. Based on the field-testing methods, a field-testing protocol is recommended for the live-load testing of historic covered timber bridges. Feasibility of the recommended protocol is also evaluated using a finite-element model analysis for a selected bridge among the tested bridges. **DOI:** 10.1061/(ASCE)CF.1943-5509.0000852. © *2015 American Society of Civil Engineers.*

Author keywords: Field testing; Live-load performance; Timber; Covered bridges; Burr arch truss; Howe truss; Queen post truss.

Introduction

The National Historic Covered Bridge Preservation Program (NHCBP), which is sponsored by the Federal Highway Administration (FHWA), aims to preserve, rehabilitate, and renovate historic covered timber bridges that were built in the early 1800s. Today, many of the nearly 880 covered timber bridges (FHWA 2005) that are still in existence in the United States are located in the northeastern regions, including Pennsylvania, Ohio, and Vermont, but are also found in large numbers in the western regions, particularly Oregon. Most of the bridges are closed to normal vehicular traffic; furthermore, a large percentage of the remaining bridges open to traffic are load posted. As such, the FHWA, the U.S. Department of Agriculture (USDA) Forest Products Laboratory, and the National Park Service (NPS) have identified the need to reliably evaluate the live-load performance of these bridges, and have sponsored a pertinent research program to establish a historic covered bridge load rating procedure derived in part through field testing. It is generally required that analytical models created by finite-element software be validated and calibrated with actual data resulting from vehicles that are allowed to pass over the bridges and then be used to determine the load ratings of the bridges under the AASHTO design trucks. By properly validating and calibrating the models, they are capable of reflecting the live-load behavior of the bridge; unfortunately, a lack of sufficient field data exists that could be used to guide the creation of such calibrated models.

A number of studies related to timber bridge performance that investigated structural performance attributes related to structural adequacy have focused on uncovered highway bridges. These attributes include lateral live-load distribution (Gilham and Ritter 1994; Fanous et al. 2011), dynamic load allowance (Le et al. 1998), live-load deflection (Hosteng et al. 2005), and fatigue life estimate (Thompson et al. 2002; Davids et al. 2005). Recently, Wacker and Groenier (2010) conducted a comparative analysis of North American and European bridge design codes for highway timber bridges, indicating that these codes have many similarities and some differences. Meanwhile, numerous recent studies for other bridge types have been performed to evaluate their structural performance (Seo et al. 2013, 2014, 2015; Seo and Hu 2015).

In contrast, a relatively small amount of research (Spyrakos et al. 1999; Lamar and Schafer 2004; Sangree and Schafer 2008) has been performed to examine the structural behavior and adequacy of historic covered timber bridges. Spyrakos et al. (1999) performed static analyses for a timber burr-arch truss bridge to capture the structural responses to dead and live loads, and to evaluate the live-load performance. However, the models were neither validated nor calibrated using field responses; as a result, the models may not be reliable for load-rating computations. Lamar and Schafer (2004)

[1]Assistant Professor, Dept. of Civil and Environmental Engineering, South Dakota State Univ., Brookings, SD 57007 (corresponding author). E-mail: junwon.seo@sdstate.edu

[2]Codirector, National Center for Wood Transportation Structures, 2711 S. Loop Dr., Suite 4700, Ames, IA 50010. E-mail: kickhos@iastate.edu

[3]Director, Bridge Engineering Center, Iowa State Univ., 2711 S. Loop Dr., Suite 4700, Ames, IA 50010. E-mail: bphares@iastate.edu

[4]Research Engineer, USDA Forest Service Forest Products Laboratory, One Gifford Pinchot Dr., Madison, WI 53726. E-mail: jwacker@fs.fed.us

Note. This manuscript was submitted on July 7, 2015; approved on October 12, 2015; published online on December 22, 2015. Discussion period open until May 22, 2016; separate discussions must be submitted for individual papers. This paper is part of the ***Journal of Performance of Constructed Facilities***, © ASCE, ISSN 0887-3828.

computationally looked into the structural behavior of two different historic covered timber bridges: the Burr arch and town-lattice truss bridges. Sangree and Schafer (2008) later carried out field tests to better investigate the Burr arch-truss bridge's behavior. A model was calibrated with the field measurements that reflected the current bridge's condition. A queen post truss bridge was also modeled and calibrated with field data for accurately assessing its structural adequacy. Unfortunately, the study examined only the global bridge deflection of the bridges. To explicitly explore the live-load performance of historic covered bridges and to reliably calibrate the models in different aspects, sufficient field measurements in terms of global and local behaviors of various types of historic covered timber bridges are needed.

To explore the actual structural behavior and the performance of historic covered bridges, a series of field tests were conducted at existing historic covered timber bridges. The tests consisted of installing a network of multiple displacement and strain sensors on the structures, and monitoring global displacements and member strains at various cross sections during passage of a known test vehicle (which met the load restrictions in place at the time). The data provided in this study can form the basis for improved instrumentation, live-load testing, and validation and calibration of analytical models, in addition to the reliable load rating computation on such bridges.

Fig. 1. Photographic overview and interior view for each of the historic covered bridge types: (a) Burr arch truss; (b) Howe truss; (c) queen post truss (images by Travis K. Hosteng)

Field-Testing Procedure

Determination of an accurate load rating for historic covered bridges using an analytical model first requires that accurate live-load performance data be obtained to calibrate the analytical model. In this paper the procedures followed during the testing of the aforementioned bridges are described. This includes the description of the selected bridges, instrumentation plan, and load vehicles and paths.

Selected Bridges

Eleven historic covered timber bridges located across the United States were selected for this study. Included in the bridges are three Burr arch–truss bridges in Indiana, four Howe truss bridges in Indiana, and four queen post–truss bridges in Vermont. These three truss types were selected because they have a large population of bridges surviving these days. The Burr arch–truss bridge is defined as a combination of an arch and multiple kingpost truss members, which consist of two diagonal members inclined to a vertical post. The Howe truss bridge is defined as a combination of vertical and diagonal members. The queen post–truss bridge is defined as a bridge coupled with two central supporting posts. Sample photographs for each bridge type are shown in Fig. 1. This figure shows that all the bridges are timber truss structures supporting their own timber deck surfaces that carry loads over an obstruction. Each through-truss bridge has a timber framing roof system, top and bottom chords with horizontal cross bracing, posts and diagonals, stringers, and floor beams. The roof system and enclosed sides have been used to preserve the individual components and joints against environmental attacks. Further detailed information for all 11 bridges is given in Table 1. For example, the Cox Ford bridge, which was constructed in 1913 and rehabilitated in 1977, is a single-span bridge with an overall roadway dimension of 58.5 × 4.8 m. This bridge is posted for a 44.5 kN load limit. Representative photographs for each of the bridges are shown in Fig. 2.

Table 1. General Information and Structural Characteristics of Selected Bridges

Bridge type	Bridge name	Bridge location	Construction year	Rehabilitation year	Structure length (m)	Structure width (m)	Posted loading (kN)
Burr arch truss	Cox Ford	Parke County, Indiana	1913	1977	58.5	4.8	44.5
	Portland Mills	Parke County, Indiana	1856	1996	39.9	4.5	—
	Zacke Cox	Parke County, Indiana	1908	1991/2002	16.9	4.7	115.7
Howe truss	Dick Huffman[a]	Putnam County, Indiana	1880	—	81.4	4.9	71.2
	James	Jennings County, Indiana	1887	—	42.7	4.8	44.5
	Rob Roy	Fountain County, Indiana	1860	1925	36.6	4.8	26.7
	Scipio	Jennings County, Indiana	1886	1984	47.5	4.8	44.5
Queen post truss	Flint	Orange County, Vermont	1845	1969	27.6	4.5	26.7
	Moxley[b]	Orange County, Vermont	1883	—	18.6	4.3	35.6
	Slaughterhouse	Washington, Vermont	1872	—	17.7	3.7	71.2
	Warren	Washington, Vermont	1879	2000	17.7	4.3	71.2

Note: All of the bridges that were selected for this study are classified as one traffic lane bridges, and most bridges are simply supported bridges with no skew supports. The structure length is measured from one side to the other side of abutment bearing, and the width is measured from out-to-out of the bridge deck.
[a]This bridge has two spans.
[b]This bridge has skew supports of 12.5°.

Fig. 2. Representative photographs for each of the historic covered bridges: (a) Cox Ford; (b) Portland Mills; (c) Zacke Cox; (d) Dick Huffman; (e) James; (f) Rob Roy; (g) Scipio; (h) Flint; (i) Moxley; (j) Slaughterhouse; (k) Warren (images by Travis K. Hosteng)

Instrumentation Plan

The instrumentation plan for each of the bridges was established initially before field testing. The plan, which includes a field inspection, was primarily intended to monitor the live-load responses of critical bridge components, including some top chords, diagonals, arches, bottom chord joints, and floor beams. To monitor and collect the live-load responses, a network of strain and displacement sensors are deployed on critical regions of various structural components. These measurements were recorded using a data acquisition system (DAS) and a laptop computer. The member strains were typically measured using the strain sensors that were attached to the members by hex-head screws and washers. Specifically, the bottom and top chords of splice joints, the midspan of the midspan floor beam, the verticals around midspan, diagonals near the bridge midspan, and various arch points were the selected locations to assess the detailed performance of each bridge. Because there are a limited number of sensors available and because of time constraints, symmetry was assumed on the trusses of each bridge and only one truss of each bridge was instrumented for the strain measurement. In addition to the member strains, global displacement measurements were made at the mid- and quarter-span points of both trusses for each bridge. These displacements were recorded with ratiometric displacement sensors mounted on tripods connected to the bridge using steel cable extensions. As an example of a typical instrumentation plan, Fig. 3 illustrates the strain and displacement sensor locations for a typical historic covered bridge field test. Fig. 4 illustrates a representative setup for the measurement of member strains and global deflections on a covered timber bridge truss.

Load Vehicles and Paths

To successfully complete a field-testing program that is both accurate and easily applicable by bridge engineers, the selection of appropriate load vehicles is a critical part of the field-testing procedure. Most of the selected bridges still exposed to normal vehicles have permissible load postings ranging from 26.7 to 115.7 kN, which limit the weight of the vehicles available for

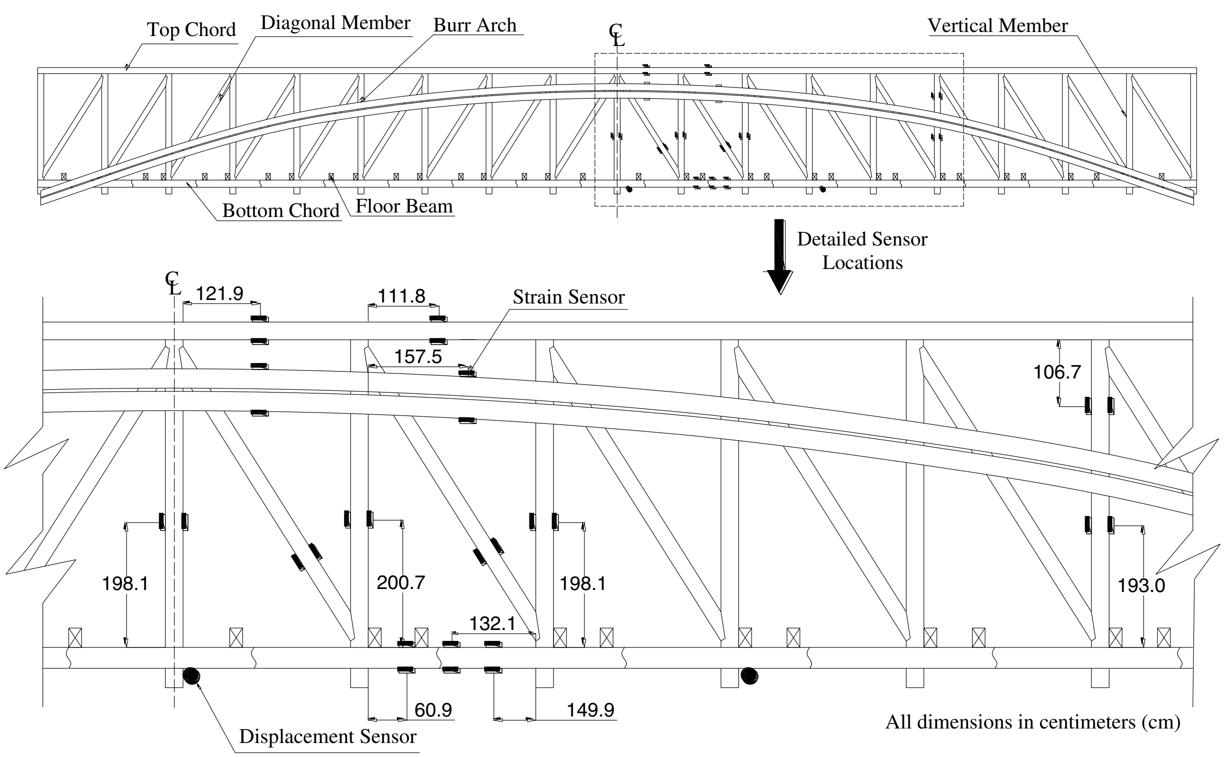

Fig. 3. Location of strain and displacement sensor instrumentation for a typical covered bridge

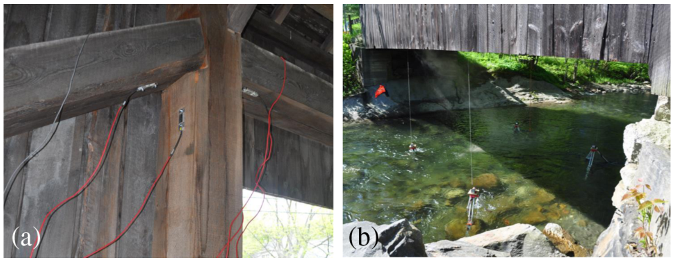

Fig. 4. Representative live-load-response measurement instrumentation setup: (a) member strains; (b) global deflections (images by Travis K. Hosteng)

Fig. 5. Representative load-testing vehicles for historic covered timber bridges: (a) sport utility vehicle; (b) pickup truck; (c) dump truck (images by Travis K. Hosteng)

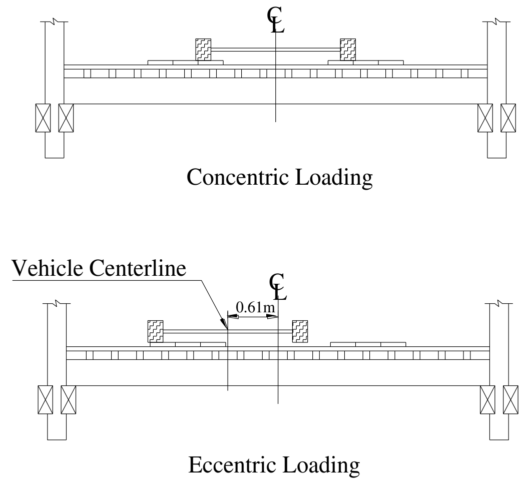

Fig. 6. Schematic of concentric and eccentric loading scenarios

use during field testing. The bridges' geometries, such as structure height and width, also impose limitations on the testing vehicle configurations applicable to the load testing. The vehicles suitable for testing covered bridges may not be similar to the AASHTO standard trucks, such as a HL-93 truck, which are required for the load rating of typical highway bridges. Based on the posting and size limitations of all of the bridges, eight vehicles with different axle weights and configurations were used for the testing. Characteristics of the trucks are listed in Table 2. Photographs for the representative testing vehicles, including a sport utility vehicle, a pickup truck, and a dump truck, are shown in Fig. 5.

During all testing, the test vehicle was driven across each bridge transversely centered on the bridge roadway. In addition to the concentric loading, eccentric loading scenarios were considered for wider bridges. The widths of the bridges vary from 3.7 to 4.9 m, as listed in Table 1. The three Burr arch–truss bridges and the four Howe truss bridges that have wider decking compared with the others were tested using both concentric and eccentric loadings. For the eccentric loading, the testing vehicle was driven across the bridge with one wheel line offset 0.61 m from the railing. The concentric and eccentric loadings are illustrated in Fig. 6.

Results and Discussion

The live-load performance of all 11 bridges was evaluated by investigating the results of visual inspection, member strains, and global deflections, independently and collectively. The detailed results and explanations for visual inspection, member stains, and global deflections for the key components of all 11 bridges are presented in the following subsections.

Visual Inspections

Before load testing the 11 bridges, each bridge was inspected according to the guidelines in the U.S. Forest Service (USFS) *Timber Bridge Manual* (Ritter 1990) and AASHTO's *Manual for Bridge Evaluation* (AASHTO 2011), to visually identify any damage or decay that could be the cause for the degradation of structural components. The inspection information helps in understanding the structural performance of each bridge tested for the field investigation. During each bridge inspection, separate as-built plans and their inspection or rehabilitation reports were carefully reviewed in addition to each site visit, to inspect all bridge components and to confirm any modifications or member replacements made to the bridge. The overall structural condition of all of the bridges was satisfactory, although some visual damage was identified and varied from slight discolorations to moderate decay and insect attack, to minor misalignments and rotations at member connections. Detailed inspection information on all 11 bridges is summarized in Table 3. For example, partial deterioration caused by insects was found at the joints or the bottom of a vertical post of the Cox Ford Bridge. The bottom chord of the bridge also has a shear failure at one splice joint, as shown in Fig. 7(a). The top layer deck of the

Table 2. Testing Vehicle Weights and Dimensions

Vehicle	Vehicle type	Front axle weight (kN)	Back axle weight (kN)	Front guage width (m)	Back guage width (m)	Axle spacing (m)	Applied bridge
A	Two-axle truck	13.4	13.4	2.0	1.8	4.0	Dick Huffman
B		13.4	13.4	1.5	1.5	2.9	Rob Roy
C		17.4	14.4	1.9	1.9	4.5	Flint and Moxley
D		17.6	28.8	1.8	1.9	4.3	Cox Ford, Portland Mills, and Zacke Cox
E		20.9	25.5	1.8	1.8	3.4	Flint, Moxley, Slaughterhouse, and Warren
F		21.9	19.0	1.8	1.8	3.4	James and Scipio
G		41.6	42.1	2.0	1.8	3.1	Cox Ford
H		47.5	68.7	2.0	1.8	3.1	Zacke Cox

Table 3. Visual Inspections of All 11 Bridges

Bridge name	Visual inspections: Overall	Joints	Vertical members	Diagonal members	Bottom chords	Top chords	Floor beams	Deck
Cox Ford	Good	Partial deterioration	Partial deterioration	Good	Some shear failure	Good	Good	Good
Portland Mills	Good	Partial deterioration	Good	Partial deterioration	Good	Good	Good	Good
Zacke Cox	Good	Partial deterioration	Good	Partial deterioration	Good	Good	Good	Good
Dick Huffman	Good	Good	Good	Partial deterioration	Good	Good	Good	Good
James	Good	Good	Good	Partial deterioration	Partial deterioration	Good	Good	Good
Rob Roy	Good	Good	Good	Good	Partial deterioration	Good	Good	Partial deterioration
Scipio	Good	Some retrofitted	Good	Some tension failure	Good	Good	Good	Good
Flint	Good	Good	Moderate deterioration	Good	Good	Good	Good	Good
Moxley	Good	Good	Good	Good	Good	Good	Good	Good
Slaughterhouse	Good	Partial deterioration	Good	Good	Good	Good	Good	Good
Warren	Good	Partial deterioration	Good	Good	Good	Good	Good	Good

Note: Visual inspections of the individual timber components were evaluated by bridge engineering judgments based on AASHTO's *Manual for Bridge Evaluation* (AASHTO 2011).

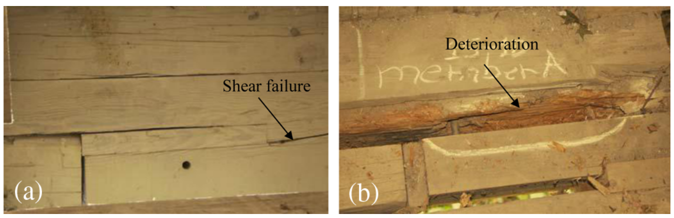

Fig. 7. Typical damage of critical structural components: (a) shear failure at one splice joint of Cox Ford bridge; (b) partial deterioration at bottom chord of Rob Roy bridge (images by Travis K. Hosteng)

Rob Roy Bridge was split from timber straps with a 5.1 cm gap. The bottom chords were found to be partially deteriorated at the southwest portion of the bridge, as shown in Fig. 7(b). Dirt, leaves, and aggregate debris were all over most bridges, which may accelerate the deterioration of critical members; thus, it is required that the bridges be periodically cleaned to avoid acute deterioration.

Member Strains

A suite of strain sensors was deployed to the critical live-load resisting members of each bridge, as shown in Fig. 3. For example, the five critical members of the Cox Ford Bridge, including top and bottom chords, vertical and diagonal truss members, and arch members, were instrumented with strain sensors. These sensors were attached to opposing faces at each location of a truss member, and the data were collected when each testing truck crossed each bridge at a crawl speed lower than 8 km/h.

The representative member strains of a typical covered bridge, in this case the Cox Ford Bridge, are shown in Fig. 8 for the concentric loading of Truck D, and Fig. 9 for the eccentric loading of Truck D, respectively. These figures show the member strains on the top and bottom faces of the top chord, bottom chord and diagonal truss, on the west and east faces for the vertical truss, and on the inner and outer arches for the arch member. As expected, these figures indicate that the eccentric loading of Truck D causes the larger strain magnitude and responses than those obtained when Truck D traveled at the centerline as a result of the interaction of combined axial loads and additional flexure resulting from eccentric loading.

As shown in Figs. 8(a) and 9(a), the strain magnitude for the top chords on the top face are similar to that for the top chord on the bottom face, although there is a significant discrepancy in terms of overall strain time history between the top and bottom face strains. The magnitudes of both the top and bottom face strains obviously increase as the testing vehicles approach the sensor locations. This trend is similarly shown in Figs. 8(b) and 9(b) for the bottom chords on the top and bottom faces. Figs. 8(c) and 9(c) show that the strain time history curves of diagonal truss strains on both the top and bottom faces are practically identical. This tendency is in line with the curves for the vertical truss strains on the west and east faces, as shown in Figs. 8(d) and 9(d). Figs. 8(e) and 9(e) show that the magnitude of strains and overall strain curves between the inner and outer arches are significantly different. Specifically, the inner arch members for both the concentric and eccentric loadings are more extensively overstrained relative to the outer arch members, even though the inner arch members behave elastically.

Based on the investigation of the member strains, it can be inferred that the vertical and diagonal members behave as axial force members, and the bottom chord acts more like a beam than an axial member, under combined bending and axial tension caused by live loads. One final implication is that the bridge exhibits elastic behavior during the passage of the vehicle, as these strains return to nearly zero when the vehicle passes over the bridge. This information can be useful to generate precise, analytical models that should be conducted in a future study to better understand the behavior of covered timber bridges. The structural behaviors of the selected bridge are similar to that of each of the other bridges. Detailed information on the member strain responses and patterns for the other bridges can be found elsewhere (Hosteng et al. 2015).

In addition to the graphical investigation of the selected bridge, the maximum and minimum values of member strains on all of the bridges subjected to the concentric and eccentric loadings are listed in Table 4. These values are used to evaluate the magnitudes of member strains for each component of individual bridges. These values indicate that most bridge components within each bridge type have a similar variation in the member strains measured during individual tests. This indicates that most bridge components in each bridge type behave similarly. Again, the strain data from the live-load testing to specific bridges can be found in the past technical report (Hosteng et al. 2015).

Global Deflections

Global deflections for all 11 bridges captured during the testing process are presented in this section. Referring to Fig. 3 for the locations of displacement sensors, these sensors are located at the

J. Perform. Constr. Facil., 2016, 30(4): 04015094

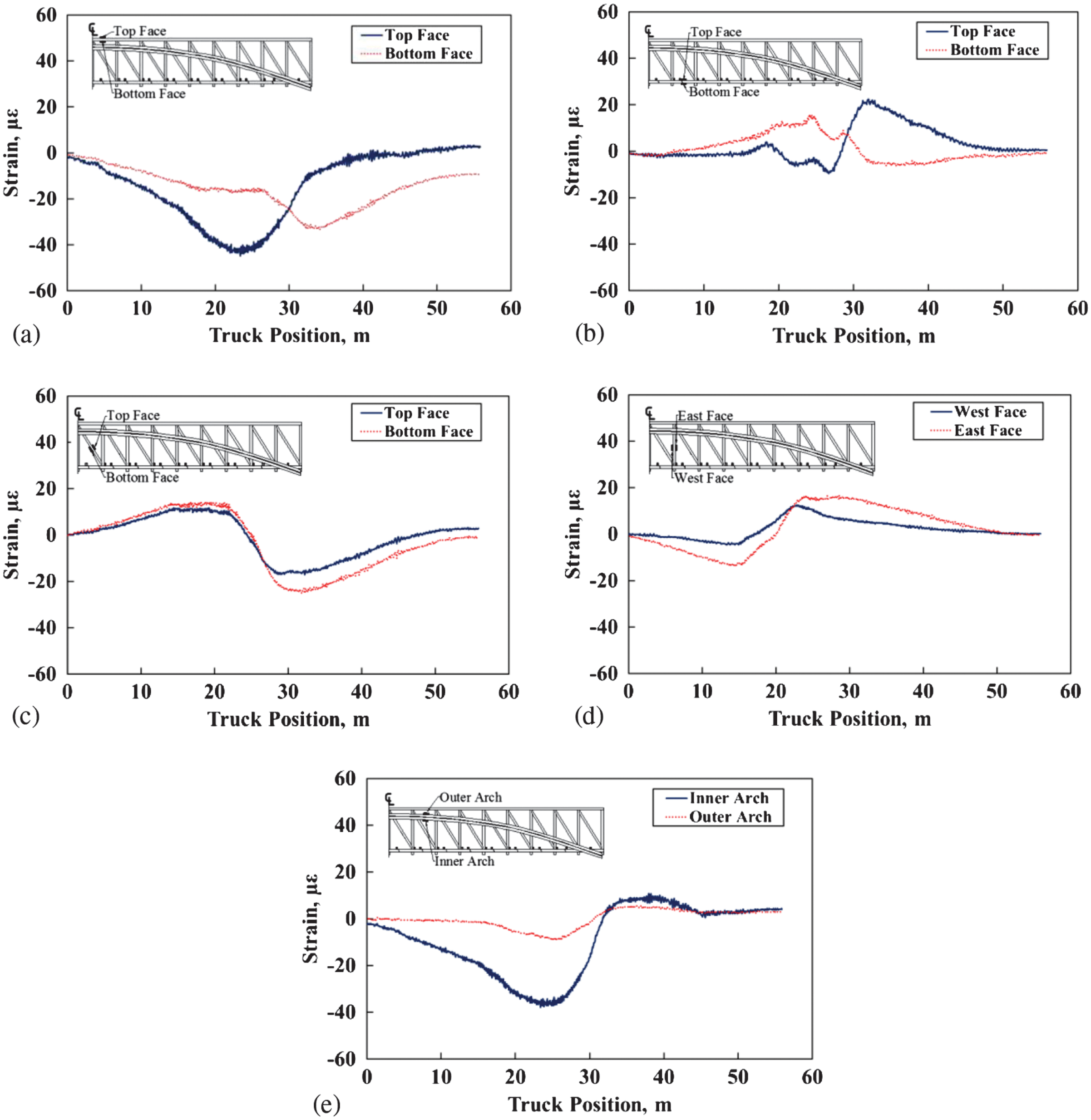

Fig. 8. Representative member strains of a typical covered bridge loaded with concentric truck loading: (a) top chord; (b) bottom chord; (c) diagonal truss; (d) vertical truss; (e) arch member

mid- and quarter-spans of the bottom chords. As an example of the global deflections for all of the bridges, the global deflection curves for the Cox Ford Bridge under the concentric and eccentric loading scenarios are selected and illustrated in Fig. 10. A notable characteristic observed in Figs. 10(a and b) is that the deflections of both truss chords at the mid- and quarter-spans resulting from the testing Truck D being centered on the longitudinal centerline of the bridge are almost identical in pattern and magnitude. This indicates that the load is equally distributed transversely across the deck to the truss chords during the passage of the truck. As observed from Figs. 10(c and d), the magnitude of deflection of the truss chord nearest the load (i.e., east truss) becomes larger than the truss chord farthest from the load (i.e., west truss) is the result of eccentric loadings; this behavior is expected when the truck is eccentrically loaded toward the east truss. This tendency is compatible with the results of the other bridges. Detailed information can be found in the past technical report (Hosteng et al. 2015).

To examine more explicitly the structural behaviors among all of the bridges in global deflection, the maximum global deflections at the mid- and quarter-spans of each bridge were compared with one another and summarized in Table 5. The deflections of each bridge were compared with the AASHTO live-load deflection limits (AASHTO 2010) that are computed as a function of span length and bridge characteristics. The AASHTO limits are included in this table, which indicates that all the deflections are satisfactory yet too conservative. It can be interpreted that the resulting load ratings that can be estimated following the current AASHTO rating procedure may be too conservative.

In addition to the maximum deflection, Table 5 also includes the ratios of the maximum deflection of one truss chord to that of the other at the mid- and quarter-spans of each respective bridge. A ratio close to or equal to 1 indicates that the live loads are transferred transversely to both chords symmetrically. The ratios for most bridges under concentric loading scenarios are close to 1,

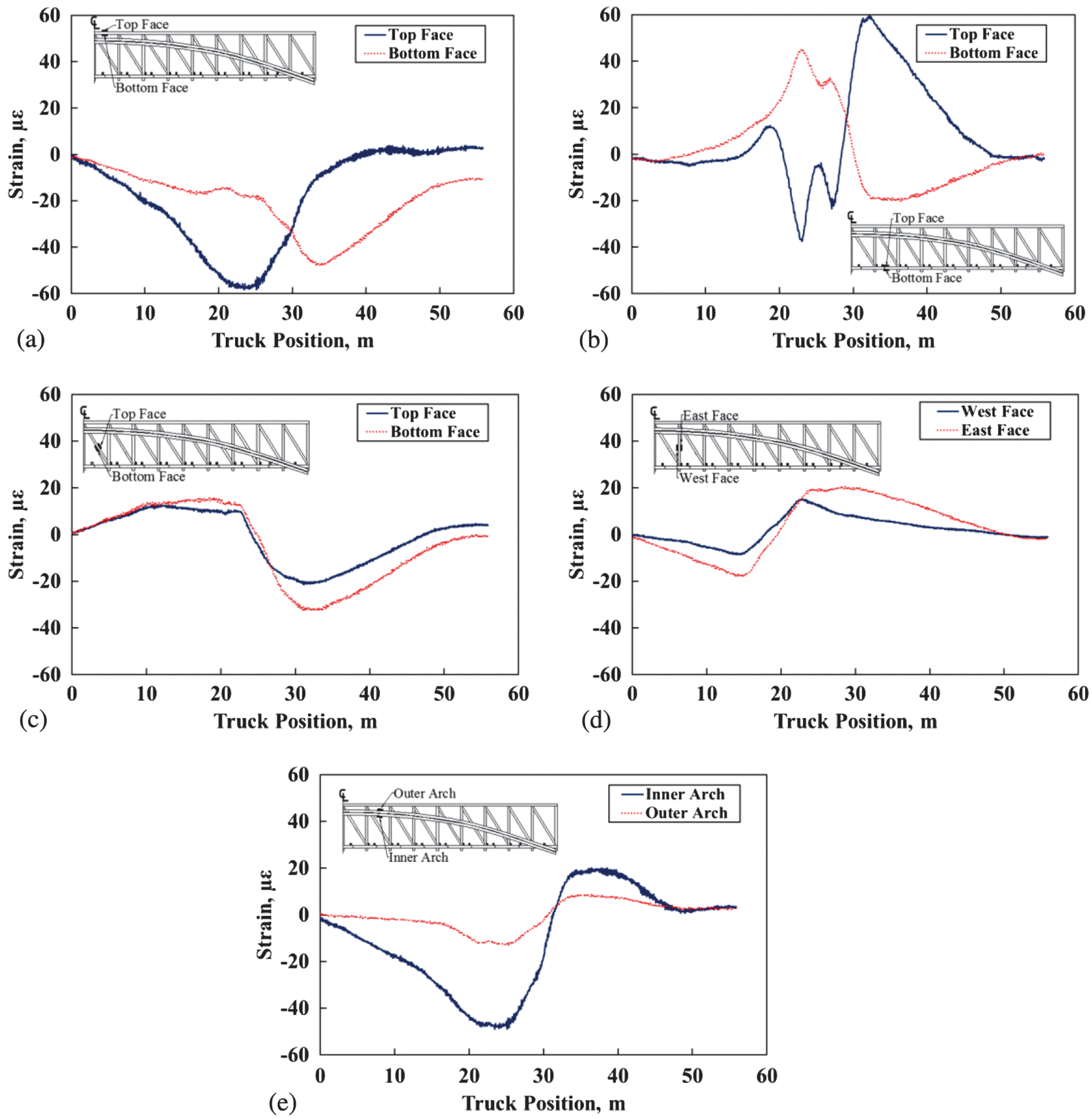

Fig. 9. Representative member strains of a typical covered bridge loaded with eccentric truck loading: (a) top chord; (b) bottom chord; (c) diagonal truss; (d) vertical truss; (e) arch member

except for the Rob Roy Bridge at only quarter-span and the Flint Bridge at both quarter- and midspans. This phenomenon for the two bridges can be attributed to the difference in structural responses between the chords, because of the extent of their dissimilar stiffness degradation that has occurred over time and their different interaction with the other components, such as roofs and walls. Additionally, the ratios for most bridges subjected to the eccentric loadings are much greater than 1 or much less than 1, because the maximum deflections of the chords adjacent to the applied load are greater than those from the other chord. Overall, the live loads can be distributed symmetrically to both chords for historical timber covered bridges, with nearly equal deflections between its chords being subjected to concentric loadings. Hence, these bridges may be simply designed and rated using conventional line girder analysis methods coupled with live distribution factors in moment and shear in longitudinal timber girders according to the AASHTO specifications (AASHTO 2010) and manual (AASHTO 2011). However, the AASHTO rating procedure that is specific to the historic timber covered bridges may be reconsidered, as the deflections under the rated loads were significantly less than the AASHTO deflection limits.

Recommended Field-Testing Procedure

Field testing of historic covered timber bridges requires that accurate and useful field data be measured to assess their live-load performance. As mentioned previously, the field data obtained from a series of live-load tests for all 11 bridges were used successfully to evaluate their live-load performance in terms of observational data, member strain, and global deflection. Hence, a recommended procedure for designing a field-test plan is made for the future testing of historic covered timber bridges. The recommended procedure is detailed in Fig. 11. The procedure consists of seven stages,

Table 4. Maximum and Minimum Field Member Strains for All 11 Bridges

		Member strain ($\mu\varepsilon$)													
	Loading	Top chord		Bottom chord		Diagonal truss		Vertical truss		Arch member		Floor beam		Stringer	
Bridge name	type	Maximum	Minimum	Maximum	Minimum	Maximum	Minimum	Maximum	Minimum	Maximum	Minimum	Maximum	Minimum	Maximum	Minimum
Cox Ford	Concentric	4.8	−44.8	22.3	−12.3	24.5	−30.9	25.7	−19.0	10.7	−38.5	—	—	—	—
	Eccentric	3.8	−63.4	59.6	−40.1	37.2	−36.6	32.7	−27.2	20.2	−55.8	—	—	—	—
Portland Mills	Concentric	5.8	−48.0	27.2	−7.1	33.2	−38.2	46.2	−32.1	13.8	−27.4	82.0	−75.4	—	—
	Eccentric	5.7	−52.2	31.6	−9.2	32.8	−43.7	57.3	−41.7	14.6	−31.0	78.4	−74.6	—	—
Zacke Cox	Concentric	3.4	−14.7	34.1	−15.1	39.4	−51.5	22.8	−10.5	2.7	−22.6	129.9	−105.5	—	—
	Eccentric	2.9	−19.1	51.1	−28.4	46.6	−62.4	29.6	−15.1	1.5	−29.5	128.6	−111.9	—	—
Dick Huffman	Concentric	0.0	−33.8	40.3	−3.9	15.4	−25.8	—	—	—	—	—	—	30.5	−23.9
	Eccentric	0.0	−27.6	50.8	−6.5	19.8	−31.6	—	—	—	—	—	—	31.6	−40.7
James	Concentric	0.0	−21.4	12.0	−12.2	9.1	−34.6	—	—	—	—	—	—	31.6	−14.2
	Eccentric	0.0	−26.9	12.4	−25.6	10.6	−52.2	—	—	—	—	—	—	45.0	−14.6
Rob Roy	Concentric	0.0	−9.5	8.5	−4.1	11.1	−13.1	—	—	—	—	—	—	18.9	−13.6
	Eccentric	0.0	−13.5	11.3	−8.3	16.0	−17.0	—	—	—	—	—	—	27.5	−25.6
Scipio	Concentric	0.0	−29.9	8.8	−10.1	7.1	−14.1	—	—	—	—	—	—	26.6	−13.0
	Eccentric	0.0	−38.0	11.3	−15.8	8.9	−17.2	—	—	—	—	—	—	34.9	−16.3
Flint	Concentric	27.6	−72.7	39.0	−46.0	28.3	−45.4	23.1	−5.3	—	—	—	—	—	—
	Eccentric	—	—	—	—	—	—	—	—	—	—	—	—	—	—
Moxley	Concentric	18.5	−68.2	82.7	42.8	21.9	−44.0	44.7	−5.6	—	—	—	—	—	—
	Eccentric	—	—	—	—	—	—	—	—	—	—	—	—	—	—
Slaughterhouse	Concentric	18.2	−87.7	79.0	−8.9	—	—	34.7	−15.3	—	—	—	—	—	—
	Eccentric	—	—	—	—	—	—	—	—	—	—	—	—	—	—
Warren	Concentric	17.6	−38.7	13.5	−1.1	29.7	−2.2	—	—	—	—	140.0	−74.2	—	—
	Eccentric	—	—	—	—	—	—	—	—	—	—	—	—	—	—

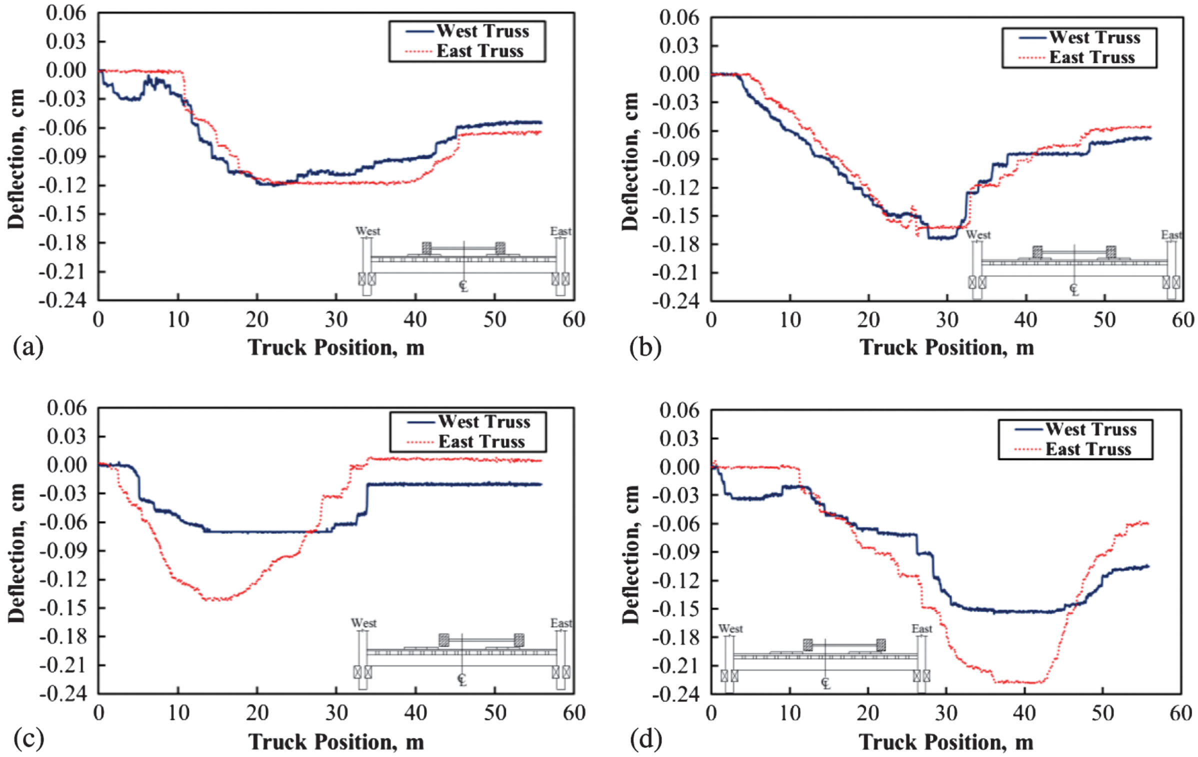

Fig. 10. Representative global deflections of a typical covered bridge: (a) concentric loading at quarter-span; (b) concentric loading at midspan; (c) eccentric truck loading at quarter-span; (d) eccentric truck loading at midspan

Table 5. Maximum Field Global Deflections at Quarter- and Midspan for All 11 Bridges and the Ratios of West Truss (or South Truss) to East Truss (North Truss)

Bridge name	Loading type	Maximum global deflection (cm)				AASHTO deflection limit (cm)	Ratio	
		Quarter-span		Midspan			Quarter-span	Midspan
		East or south	West or north	East or south	West or north		East/west or south/north	East/west or south/north
Cox Ford	Concentric	−0.05	−0.05	−0.07	−0.06	−13.76	1.03	1.09
	Eccentric	−0.03	−0.05	−0.06	−0.09	−13.76	0.55	0.68
Portland Mills	Concentric	−0.13	−0.12	−0.19	−0.16	−9.40	1.15	1.19
	Eccentric	−0.17	−0.11	−0.29	−0.19	−9.40	1.63	1.54
Zacke Cox	Concentric	−0.08	−0.06	−0.09	−0.07	−3.97	1.25	1.24
	Eccentric	−0.10	−0.04	−0.13	−0.03	−3.97	2.34	4.75
Dick Huffman	Concentric	−0.30	−0.29	−0.45	−0.45	−9.57	1.01	1.00
	Eccentric	−0.20	−0.38	−0.33	−0.57	−9.57	0.54	0.58
James	Concentric	−0.23	−0.25	−0.27	−0.30	−10.04	0.89	0.88
	Eccentric	−0.14	−0.35	−0.17	−0.42	−10.04	0.39	0.40
Rob Roy	Concentric	−0.13	−0.05	−0.14	−0.11	−8.61	2.94	1.25
	Eccentric	−0.06	−0.09	−0.07	−0.17	−8.61	0.71	0.39
Scipio	Concentric	−0.08	−0.07	−0.26	−0.21	−11.17	1.27	1.24
	Eccentric	−0.05	−0.13	−0.18	−0.29	−11.17	0.37	0.60
Flint	Concentric	−0.12	−0.21	−0.12	−0.19	−6.50	0.55	0.61
	Eccentric	—	—	—	—	−6.50	—	—
Moxley	Concentric	−0.14	−0.14	−0.10	−0.12	−4.37	1.04	0.90
	Eccentric	—	—	—	—	−4.37	—	—
Slaughterhouse	Concentric	−0.23	−0.26	−0.40	−0.37	−4.17	0.86	1.10
	Eccentric	—	—	—	—	−4.17	—	—
Warren	Concentric	−0.06	−0.06	−0.11	−0.10	−4.17	1.03	1.09
	Eccentric	—	—	—	—	−4.17	—	—

including visual inspection, instrumentation setup, instrumentation layout, installation techniques, test load path selection, test vehicle selection, data collection/analysis, instrumentation, and vehicular loading. Each stage is described as follows.

Stage 1 is to perform a *visual inspection* of a target historic timber covered bridge. The visual inspection is a critical step for the accurate assessment of the in situ structural conditions of the target bridge before the field testing. It is recommended that such bridges

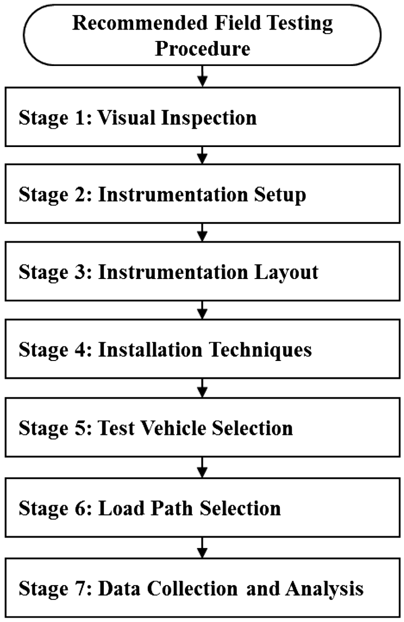

Fig. 11. Recommended procedure for designing a field-test plan for historic covered timber bridges

be visually inspected following the guidelines in the USFS *Timber Bridge Manual* (Ritter 1990) and AASHTO's *Manual for Bridge Evaluation* (AASHTO 2011) for the identification of any deteriorating bridge components. During the visual inspection, various documentation such as as-built plans, historical inspection, and rehabilitation reports should be referred along with a site visit for any member modifications or replacements check. In addition to the document reviews, on-site measurements of specific components such as truss and deck members should be made to obtain their configurations in this stage.

Stage 2 is to start with an *instrumentation setup* for live-load testing. Because these bridges are historic landmarks, all effort must be made to ensure that the bridge preservation is made in terms of structural and functional integrity during the entire process of instrumentation and testing. For example, the sensors to be used for live-load testing should provide a method of attachment to the structure and/or members that is as noninvasive and nondestructive to the member and the bridge as possible. Another possible way to avoid any damage that may occur during instrumentation and data collection is to use non-contact-based sensors (e.g., optical detection with laser sensors), which are able to measure precisely the global displacements of these bridges subjected to the passage of testing vehicles. However, accuracy in the measurements using these sensors, particularly laser sensors, is considerably affected by surface conditions, such as impediments like dirt and dust on the bridges. Therefore, it is necessary to remove such contamination when monitoring the structural quantities of the bridges using such sensors. The plan intended to monitor the live-load behaviors on such bridges should include measurements of at least both the strain and displacement quantities for critical structural components, including some top chords, diagonals, arch rings, bottom chords joints, and floor beams.

Stage 3 is to establish an adequate *instrumentation layout* for live-load testing. The layout should be designed appropriately for the successful testing of historic timber covered bridges. As stated previously, the live-load testing for all 11 bridges required a comprehensive instrumentation plan to obtain accurate and useful data that would capture the structural live-load behavior on such bridges. Based on the instrumentation plan for all 11 bridges, the following key areas are the focus of the instrumentation layout: strain sensor locations including the top and bottom chords, the diagonals, the arch rings, the bottom chord joints and floor beams, and the displacement sensor locations that encompass the mid- and quarter-span of the truss, which is the main load-carrying member of the bridges.

Stage 4 is to finalize the instrumentation plan by considering the *installation techniques*. Because these bridges are made entirely of timber, timber properties such as the modulus of elasticity, moisture content, and density of timber may vary widely from member to member, and even within an individual member. Furthermore, the fiber makeup of timber coupled with any defects (e.g., knots, checks, splits) located in the member often result in a variable stress distribution on any given cross section. The sensors selected in Stage 3 need to be evaluated to determine whether they are sensitive enough to collect appropriate data without being negatively affected by local defects or variations in installation technique. Within this stage, accurate information of timber properties and the extent of its degradation can be obtained from the review of historical inspection and rehabilitation reports, in addition to visual inspection. In situ sampling of timbers can be also performed to determine their species and to detect any decay.

Stage 5 is to *select test vehicles*. The vehicle selection is an important factor for the testing of historic covered timber bridges. Numerous historic covered timber bridges that are still open to traffic have legal load postings (e.g., 44.5 kN) that limit the size in terms of weight of the vehicle, and can be used securely for load testing. The configuration of covered timber bridges in terms of their entrance height and width between the trusses may also be used for the load testing. The testing vehicle necessary for a specific covered bridge testing may not resemble a typical highway-type truck such as HS20 trucks, which are used as standard live-load trucks for designing and rating highway bridges. Bridge posting and size limitations may require the use of smaller dump trucks, heavy-duty pickup trucks, or even small to large-size sport utility vehicles.

Stage 6 is to *select load paths*. The inherent narrow width of typical historic covered timber bridges range from 4.3 to 6.1 m, which limits the transverse load paths that may be evaluated during testing. At a minimum, a concentric loading scenario should be evaluated, which involves the vehicle being centered over the longitudinal centerline of the bridge. As the transverse load–distribution characteristics on such bridges under various loading scenarios are required, the addition of an eccentric load case, which involves the load truck being driven across the bridge with one wheel line offset 0.61 m from the railing, may be provided when the structure possesses adequate width such that the placement of the truck in the eccentric load path is sufficiently different than its placement in the concentric load path.

Stage 7 is to *collect and analyze data* in a technical and scientific manner. The data collection and analysis is the final important process for live-load testing. In fact, the level of instrumentation plan may vary significantly depending on the data collection process, so that the process may be determined adequately before the completion of the instrumentation plan. For example, if the testing aims to capture only live-load-distribution characteristics of timber bridges, the testing requiring a more simple type of sensor than testing to evaluate global and local structural behaviors of bridges is needed. To generally evaluate the live-load performance of historic covered bridges comparable with the tested 11 bridges, it is required that the structural behaviors of critical bridge components be appropriately captured when a testing vehicle selected in the

J. Perform. Constr. Facil., 2016, 30(4): 04015094

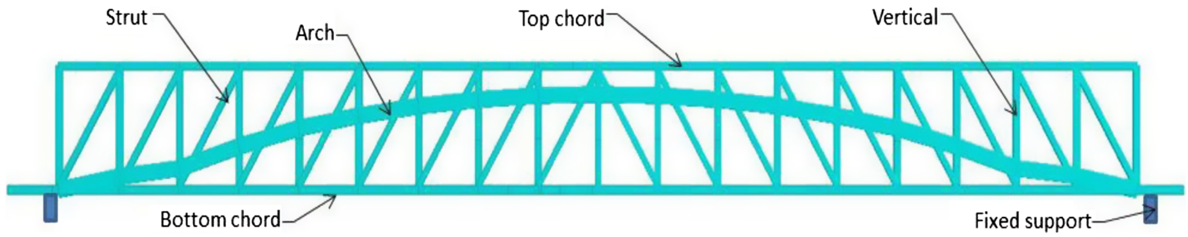

Fig. 12. Finite-element model of a typical covered bridge

Table 6. Sectional and Material Properties of the Cox Ford Bridge

Bridge component	Width (cm)	Depth (cm)	Elastic modulus (MPa)
Top chord	23.20	28.04	15,306.37
Bottom chord	35.56	33.02	12,755.30
Arch	27.94	60.96	8,273.71
Verticals	22.86	27.94	15,306.37
Diagonals	24.13	24.13	12,410.57

previous stage crosses a bridge at a crawl speed (approximately 8.05 km/h). Strains for the top and bottom chords, vertical and diagonal truss members, and arch members and deflections for the mid- and quarter-span of both truss chords should at least be collected for the accurate and efficient live-load performance assessment of such bridges. Based on the recommended field-testing procedure, multiple live-load tests for all 11 bridges were performed successfully to evaluate their field live-load characteristics adequately.

Cursory Field-Testing Procedure Evaluation

The feasibility of the recommended field-testing procedure that was validated with its application to all 11 tested bridges was also evaluated numerically by comparing the field results with the analytical results for a typical covered timber bridge. A finite-element model of the Cox Ford Bridge that was selected for this numerical substantiation was generated using *STAAD* software following a

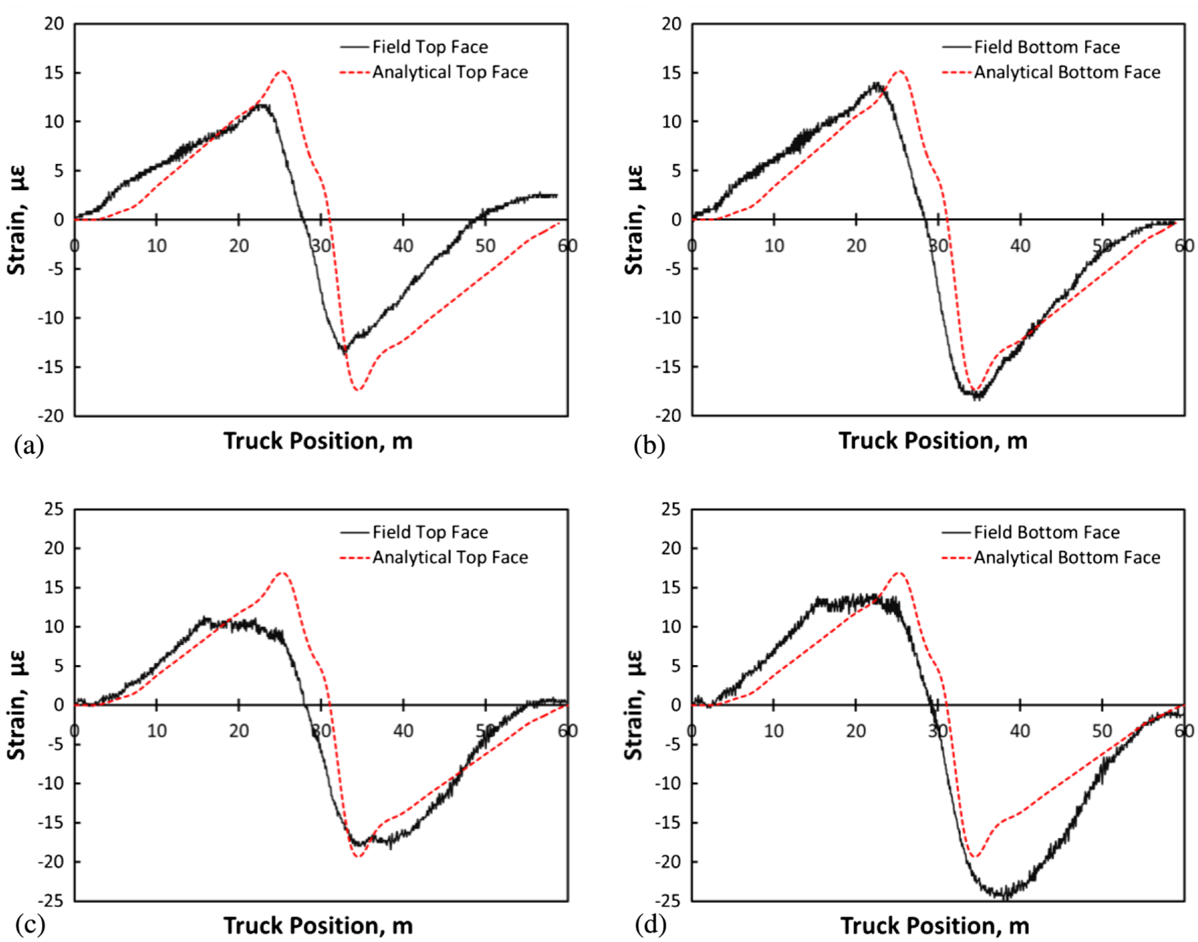

Fig. 13. Representative comparison plots between strain curves for a typical covered bridge: (a) top face of diagonal truss under concentric loading; (b) bottom face of diagonal truss under concentric loading; (c) top face of diagonal truss under eccentric loading; (d) bottom face of diagonal truss under eccentric loading

J. Perform. Constr. Facil., 2016, 30(4): 04015094

general linear-elastic modeling approach. The software was selected because of its ease and extensive use in the timber bridge engineering community. Modeling the bridge began by generating a fundamental truss model representing the structure, using truss elements for all of the critical members, pinned supports, and pinned connections between all members. A schematic of the finite-element model is portrayed in Fig. 12. For convenience, the extended portion of the arch rings below the bottom chord was neglected. The geometric and material properties of the model are listed in Table 6.

For the concentric-load cases, it was assumed that 50% of the total load truck weight was distributed to each truss for refining the finite-element model. In addition to the concentric load cases, an eccentric load case was simulated with the testing truck being offset 0.61 m toward the near truss (Fig. 6). Assuming proper lateral load distribution and placing the truck eccentrically, the percent of load to the near truss is calculated to be approximately 55% of the total load truck. This was taken as the load distributed to the near truss for evaluating the accuracy of the refined model. These assumptions for both the concentric and eccentric load cases were verified based on the evaluation of the live-load deflection field test results (Table 5). The selected testing trucks listed in Table 2 were applied to the model as they crossed the bridge during the field test. Member strains on the top and bottom surfaces of the critical members of all strain sensors were calculated using the recommended procedure. Representative comparison plots are illustrated in Fig. 13, comparing the top and bottom field strains with the analytical strains for the primary load resisting components of the bridge under either concentric or eccentric loading scenarios. The simulations are proven to have yielded reasonable agreement between the field and analytical results for both the concentric and eccentric load cases. Hence, the model created and refined with field data obtained in accordance with the recommended field-testing procedure can be used efficiently for the load-rating calculation of the selected bridge.

Conclusions

To better understand the live-load condition of historic covered timber bridges, which are considered to be the most iconic bridges constructed in the United States in the early 1800s, a series of live-load tests were performed on 11 single-span, historic covered timber bridges. The three groups of bridges chosen for live-load testing included (1) three Burr arch–truss bridges in Indiana, (2) four queen post–truss bridges in Vermont, and (3) four Howe truss bridges in Indiana. Before the live-load tests, all 11 bridges were inspected to document the truss member sizes and orientations, and to investigate any damage causing the degradation of structural components. Each bridge was then instrumented with a network of displacement and strain sensors for the collection of structural performance data that could be used as the basis to evaluate the structural behavior of the bridge subjected to vehicular loads. Once the instrumentation was installed on the bridge, a test vehicle of known weight that met the load-posting requirement of the bridge was driven across the bridge at a crawl speed. The strain and deflection data were collected from the application of the live load and used for the evaluation of the structural response of the bridge. Substantial results from the testing of all 11 bridges include the following:

1. A field inspection of each bridge indicated that visual damage varied from slight discolorations to moderate decay and insect attack. The overall structural health condition of all 11 bridges was satisfactory, although partial deterioration from insect attack or separate timber straps with a minor gap were found at some structural components for several bridges, especially the Cox Ford Bridge, which had somewhat moderate degradation at the joints and bottom of vertical posts.
2. A structural component–level strain data investigation of each bridge revealed that the structural performance of each component subjected to concentric and eccentric vehicular loadings behaved elastically. As expected, the eccentric loading causes the larger strain magnitude and responses of each bridge than those obtained from the concentric loading, attributable to the interaction of combined axial loads and additional flexure resulting from eccentric loadings.
3. The maximum global deflections at the mid- and quarter-spans of each bridge were compared with the AASHTO live-load deflection limits (AASHTO 2010), indicating that all of the deflections are satisfactory. A comparison between one and the other supporting truss chords in terms of global deflections indicates that the deflections between a pair of chords for each of the bridges subjected to the testing truck being centered on the longitudinal centerline are almost identical in terms of pattern and magnitude. This indicates that approximately equal live loads are able to be distributed transversely across the deck to both chords during the passage of the truck. Therefore, these bridges can be easily designed and rated using conventional line girder analysis methods coupled with live distribution factors in longitudinal timber girders following the AASHTO specifications (AASHTO 2010) and manual (AASHTO 2011).
4. A recommended procedure for designing a field-test plan was presented based on the live-load performance testing for all 11 bridges. The procedure involves visual inspection, instrumentation plan with vehicle loading scenarios, and data collection and analysis. According to the recommended procedure, the live-load testing of potential historic covered timber bridges deemed as historic landmark structures in the United States can be conducted successfully to obtain adequate and useful data without any damage to the structures.
5. The feasibility of the recommended testing procedure was evaluated by comparing field to simulation results for a typical covered timber bridge. The bridge was generated using commercially available finite-element software and calibrated with field data obtained from the testing procedure. The findings revealed that the model efficiently replicated the field data for the truck positions, although slight discrepancies between the field and simulation results were observed. Therefore, the model coupled with field data from the recommended procedure has the potential to produce load ratings for the bridge in an effective manner.

Given the historic nature and unique geometrical features of these bridges, a key benefit of the field results obtained from this study is for use in service-load-rating assessment of a population of historic covered timber bridges with irregular configurations. In future work, the structural characteristics provided from all of the tested bridges will be used to generate analytical models using commercially available finite-element software, and to calibrate them against the field data. The calibrated models will be used to accurately assess the load-carrying capacities of all 11 bridges being subjected to service loads according to the AASHTO manual (AASHTO 2011).

Acknowledgments

This research was sponsored by the Federal Highway Administration and the USDA Forest Products Laboratory (FPL) under the National Historic Covered Bridge Preservation Program. The authors especially thank Doug Rammer from the FPL for his cooperation and assistance during the field testing of the covered bridges.

References

AASHTO. (2010). *AASHTO LRFD bridge design specifications*, Washington, DC.

AASHTO. (2011). *AASHTO manual for bridge evaluation*, Washington, DC.

Davids, W., Dagher, H., Richie, M., and Sanchez, O. (2005). "Fatigue of glulam beams with fiber-reinforced polymer tension reinforcing." *Forest Prod. J.*, 55(1), 93–101.

Fanous, F., May, J., and Wipf, T. (2011). "Development of live-load distribution factors for glued-laminated timber girder bridges." *J. Bridge Eng.*, 10.1061/(ASCE)BE.1943-5592.0000127, 179–187.

FHWA (Federal Highway Administration). (2005). *FHWA covered bridge manual*, McLean, VA.

Gilham, P. C., and Ritter, M. (1994). *Load distribution in longitudinal stringer-transverse deck timber bridges*, USDA Forest Service, Forest Products Laboratory, Madison, WI.

Hosteng, T., et al. (2015). *Covered bridge rating through load testing—final report*, USDA, Washington, DC.

Hosteng, T., Phares, B., Wipf, T., Ritter, M., and Wood, D. (2005). "Live load deflection performance of glued laminated timber girder bridges." *Transp. Res. Rec.*, 1928, 174–182.

Lamar, D. M., and Schafer, B. W. (2004). "Structural analyses of two historic covered wooden bridges." *J. Bridge Eng.*, 10.1061/(ASCE)1084-0702(2004)9:6(623), 623–633.

Le, X., Kainz, J., Peterson, M. L., and Landisic, E. N. (1998). *Smart timber bridges for in-situ evaluation*, USDA Forest Service, Forest Products Laboratory, Madison, WI.

Ritter, M. A. (1990). *Timber bridges-design, construction, inspection, and maintenance*, USDA, Washington, DC.

Sangree, R. H., and Schafer, B. W. (2008). "Field experiments and numerical models for the condition assessment of historic timber bridges: Case study." *J. Bridge Eng.*, 10.1061/(ASCE)1084-0702(2008)13:6(595), 595–601.

Seo, J., Czaplewski, T. M., Kimn, J. H., and Hatfield, G. (2015). "Integrated structural health monitoring system and multi-regression models for determining load ratings for complex steel bridges." *Measurement*, 75, 308–319.

Seo, J., and Hu, J.-W. (2015). "Influence of atypical vehicle types on girder distribution factors of secondary road steel-concrete composite bridges." *J. Perform. Constr. Facil.*, 10.1061/(ASCE)CF.1943-5509.0000566, 04014064.

Seo, J., Phares, B., Lu, P., Wipf, T., and Dahlberg, J. (2013). "Bridge rating protocol using ambient trucks through structural health monitoring system." *Eng. Struct.*, 46, 569–580.

Seo, J., Phares, B., and Wipf, T. (2014). "Lateral live-load distribution characteristics of simply supported steel girder bridges loaded with implements of husbandry." *J. Bridge Eng.*, 10.1061/(ASCE)BE.1943-5592.0000558, 04013021.

Spyrakos, C. C., Kemp, E. L., and Venkatareddy, R. (1999). "Seismic study of an historic covered bridge." *Eng. Struct.*, 21(9), 877–882.

STAAD Pro V8i [Computer software]. Bentley Systems, Exton, PA.

Thompson, R. J. H., Ansell, M. P., Bonfield, P. W., and Dinwoodie, J. M., (2002). "Fatigue in wood-based panels. Part 1: The strength variability and fatigue performance of OSB, chipboard and MDF." *Wood Sci. Technol.*, 36(3), 255–269.

Wacker, J. P., and Groenier, J. S. (2010). "Comparative analysis of design codes for timber bridges in Canada, the United States, and Europe." *Transp. Res. Rec.*, 2200, 163–168.

J. Perform. Constr. Facil., 2016, 30(4): 04015094